

A Three-Player GAN for Super-Resolution in Magnetic Resonance Imaging

Qi Wang, Lucas Mahler, Julius Steiglechner, Florian Birk, Klaus Scheffler, Gabriele Lohmann

Abstract— Learning based single image super resolution (SISR) task is well investigated in 2D images. However, SISR for 3D Magnetic Resonance Images (MRI) is more challenging compared to 2D, mainly due to the increased number of neural network parameters, the larger memory requirement and the limited amount of available training data. Current SISR methods for 3D volumetric images are based on Generative Adversarial Networks (GANs), especially Wasserstein GANs due to their training stability. Other common architectures in the 2D domain, e.g. transformer models, require large amounts of training data and are therefore not suitable for the limited 3D data. However, Wasserstein GANs can be problematic because they may not converge to a global optimum and thus produce blurry results. Here, we propose a new method for 3D SR based on the GAN framework. Specifically, we use instance noise to balance the GAN training. Furthermore, we use a relativistic GAN loss function and an updating feature extractor during the training process. We show that our method produces highly accurate results. We also show that we need very few training samples. In particular, we need less than 30 samples instead of thousands of training samples that are typically required in previous studies. Finally, we show improved out-of-sample results produced by our model.

Index Terms— Generative adversarial networks, stable training, Magnetic resonance imaging, super-resolution

I. INTRODUCTION

High-resolution MR images are crucial for obtaining a detailed view of anatomical structures and are essential for downstream MRI analysis. However, the acquisition of high-resolution (HR) MRI is labor-intensive and susceptible to motion artifacts during the scanning process. Furthermore, reducing scan time often results in lower spatial resolution and the loss of fine details in the image structure. Therefore, the research focus in deep learning has shifted towards the Single Image Super Resolution (SISR) task, which aims to recover high-resolution MR images from lower-resolution images of the same subject.

Julius Steiglechner and Florian Birk are supported by the Deutsche Forschungsgemeinschaft (DFG – German Research Foundation). The grant number for J.S. is DFG LO1728/2-1 and the grant number for F.B. is DFG HE 9297/1-1.

Qi Wang, Lucas Mahler, and Julius Steiglechner are with Max Planck Institute for Biological Cybernetics, Tübingen, Germany (e-mail: qi.wang@tuebingen.mpg.de; lucas.mahler@tuebingen.mpg.de; julius.steiglechner@tuebingen.mpg.de).

Florian Birk, Klaus Scheffler and Gabriele Lohmann are with both Max Planck Institute for Biological Cybernetics and University Hospital of Tübingen, Tübingen, Germany (e-mail: florian.birk@tuebingen.mpg.de; klaus.scheffler@tuebingen.mpg.de; lohmann@tuebingen.mpg.de)

As a result of the curse of dimensionality and limited availability of data, training an SISR model on 3D medical images is an ill-posed problem that is more challenging than training on common 2D images. Medical images, such as brain MRI, contain anatomical information in all three dimensions, making the task of SISR on 3D volumetric MRI the focus of this paper.

In the 2D domain, several studies have been conducted to achieve high image fidelity in SISR tasks, e.g. [4], [14], [16], [35]. Most of these models are trained using GAN architecture [6], which is a popular and powerful architecture in generative models. Recently, other models such as score-matching models [32], diffusion probability models [10], and transformers [5] have also been used to produce SR results with advanced image quality in both metric scores and visual fidelity. In the 3D MRI domain, some of these models have been re-implemented, with the majority of them being GANs [3], [26], [33], [36], and they continue to improve the state-of-the-art performance.

However, GAN training is known to be very unstable, sensitive to parameter changes, and requires careful design of the architecture, especially in the high dimension space and with deep architecture design. Wasserstein variations of GAN [22] [7] are the most effective and popular methods implemented in training SR models in the 3D MRI domain. Despite their effectiveness, we have observed that the results from the WGAN (or WGANGP) variations (e.g. DCSRN [3]) are often prone to blur, which can be a consequence of their convergence to suboptimal points or oscillating around the global optimum [23], [37].

In this paper, we propose to tackle this problem by introducing instance noise to the model and incorporating relativistic GAN loss [13] into a three-player adversarial training [17] framework. Our proposed model exhibits stable training dynamics and produces high-quality results, demonstrating superior generalisation performance on previously unseen data compared to other models.

In the field of SR models on MRI, it is common practice to train on a fixed dataset without variation in modality or machine type. This approach can lead to limitations in model generalisability and domain-specific biases. However, in the case of brain MRI images, the shared content among images allows for effective inductive bias. This allows the model to learn informative features even with limited training data.

To test this assumption, we trained a model on a single subject and successfully recovered the HR image. We further

observed that training on dozens of samples did not sacrifice performance and our model exhibited superior generalisability on out-of-distribution (OOD) data, indicating minimal mode collapse in the GAN. To summarise, our contributions in this work are listed:

- we show empirically that our model exhibits better convergence towards the global optimum than other models on high-dimensional data (*e.g.* 3D brain MRI).
- we show that the performance of our model remains robust even with a limited number of training samples.
- we show our model can generalize well to datasets of different modalities and resolutions.

II. RELATED WORK

A. Super-Resolution in MR Images

Learning based SISR has been actively studied in both 2D and 3D images. In a SISR task, the neural network aims to learn a non-linear mapping from the low resolution image (LR) to its high resolution (HR) reference. This is particularly suited to the convolutional neural network (CNN) learning capability, as demonstrated in previous studies [4], [16], [35], [40].

In the 2D domain, SRCNN [4] was the first to propose training an end-to-end CNN architecture to capture the feature used for mapping LR to HR, demonstrating that the deep learning methods surpass the traditional SISR methods by a large margin. Subsequently, many architectures have been proposed to improve the performance of the models on SISR task. SRGAN [16] was the first to employ a GAN framework, skipping connection [9], and perceptual loss [12] to achieve better perceptual quality of the produced SR images [16]. The VDSR [14] model improved performance by using a deeper architecture that allowed larger model capacity. RCAN [40] achieved superior performance by using channel attention and more layers to train an efficient SR network. ESRGAN [35] combined many efficient modules, including a pretrained feature extractor and relativistic GAN loss [13], to achieve SR results with high fidelity. Different from ESRGAN which used a frozen pretrained feature extractor, SPSR [20] updated a third module to extract the gradient of the image as an additional constrain to generate higher fidelity results. Recently, transformers [5] [19] have been incorporated to perform *state-of-the-art* quality in the SISR task. As a novel approach, diffusion models [32] [27] are adopted to generate realistic and high quality data, with a stable training process and achieve better metric scores. These methods are all dominant in 2D SISR tasks, providing *state-of-the-art* image quality while requiring large amounts of training data as well.

Many of these studies have inspired the development of models for SISR in medical imaging domain, some of which have achieved superior performance in SISR task. In the 2D MR image domain, [39] has used squeeze-excitation attention network to achieve remarkable super-resolution results in 2D MRI, while [18] adopted a transformer architecture to achieve superior image quality in a multiscale network. Despite the successful implementations in the 2D MR images, downstream analysis typically requires 3D volumes of MR images. Simply stacking 2D slices of SR results to create a 3D volume can lead

to undesired artefacts along the cross-plane axes. Therefore, implementing a 3D model can directly outperform 2D models [26].

This paper will focus only on 3D MR image training. Most of the novel architectures have not been adapted to 3D MRI data, due to the high dimensionality and lack of data. Thus, especially for 3D MRI domain, the GAN category remains the mainstream training method, given its efficiency and high performance. An initial work by Pham et al. [26] discussed the implementation of CNN models on 3D MRI data for SISR tasks, demonstrating the advanced SR results produced by neural networks over traditional interpolation methods. In Chen et al. [3], the author combined WGAN training with densely connected residual blocks and reported prominent image quality. While in [36], the authors used implicit neural representation to realise SR by generating images at an arbitrary scale factor. In [33], the authors proposed to use image gradient as a knowledge prior for the SR task, for a better matching to local image patterns.

Although many of these studies successfully produced SR results, they are mainly constrained to the same modality or imaging sequence as the training dataset. Also the quality of the reconstruction is sometimes limited.

B. Stabilized Generative Adversarial Networks

As was described above, GANs play an essential role in SISR. Typically, a GAN model consists of two models that compete adversarially against each other during the training process. In a standard GAN model, the generator network produces synthetic results that are as indistinguishable as possible from the real samples, while the discriminator network tries to identify whether the generated results are different from the real training samples or not.

The objective function of the model is commonly referred to as the *mini-max* game. During the training, the generator aims to maximise the probability of the discriminator classifying its generated samples as real, while the discriminator aims to minimise the probability of incorrectly classifying the generated samples as real.

Due to the non-concave and non-convex optimisation property of GAN, it can be challenging to train and converge to the global optimum. One of the main causes of this is imbalanced training, where the discriminator converges too quickly, hindering the generator's ability to learn meaningful features. Much effort has been put into both stabilising training and improving convergence to the global optimum [13] [2] [23] [37] [22] [7] [24]. These modifications can be roughly categorised into four types: objective function, normalization layers, gradient regularization, and instance-wise regularization. One approach to stabilizing GAN training is weight clipping, coupled with the use of Wasserstein loss function, which was proposed in [22]. This approach was further improved in [7] by mixing both real and generated data as input for the discriminator, but still did not guarantee convergence to the optimum. In [24], spectral normalization layers were added to improve stability, while in [2], orthogonal regularization was used to improve performance, stability,

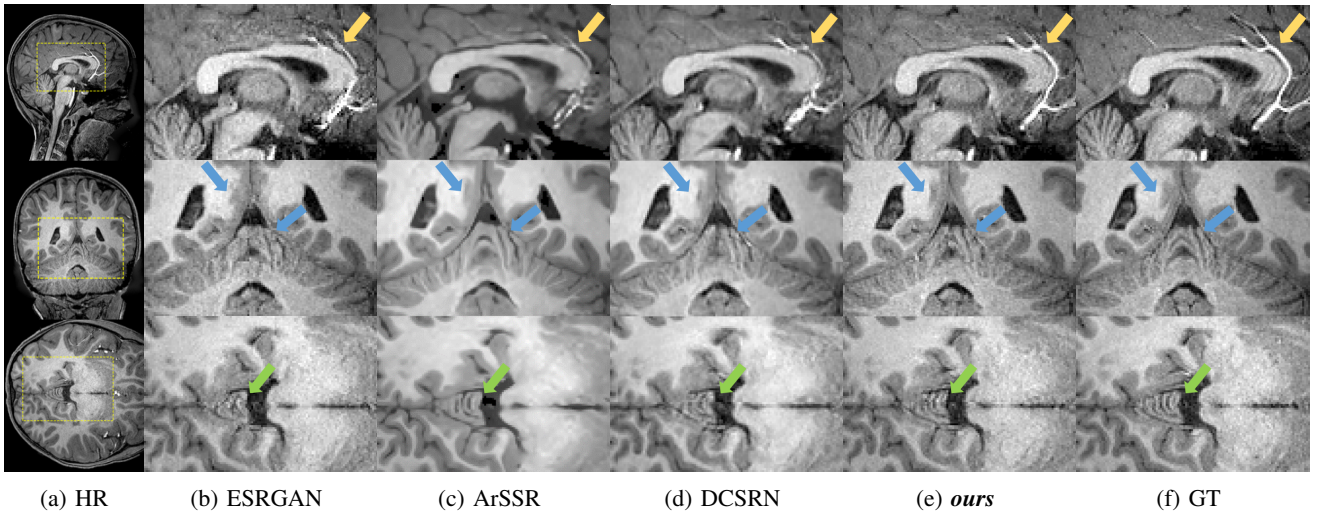


Fig. 1: Qualitative comparison on an exemplary subject using different models with a $\times 2$ resolution upscale. (a) shows the High-resolution ground truth(HR) of whole brain MRI, where the *yellow dashed box* highlights the location of the zoom-in views. The zoom-in views in subfigure(b) - (f) depicts the SR results generated by the following models: ESRGAN [35], ArSSR [36], DCSRN [3], **ours**, and GT, in sub-figure(b) - (f) respectively. Our results show the best visual quality and the most detailed recovery of the GT.(Distinguishable differences are marked by *orange*, *blue* and *green* arrows in the sub-figures(b)-(f)).

and scaling of the model. Mescheder et al. [23] conducted a theoretical investigation into the convergence properties of different GAN regularizations and found that weight-clipping GAN [7], [22] as well as the standard GAN [6] do not lead to convergence, but instead to local oscillations. This was further investigated by Xu et al. [37] from the perspective of control theory, where Xu et al. showed that convergence of Dirac GAN can be achieved by close-loop controlling. Amongst these prevailing regularizations, adding instance noise is shown to be the simplest and a computationally cheap way of stabilising the training, ensuring convergence, and providing high-quality image generation [23] [31].

III. OUR APPROACH

Regarding the model design, we constructed a GAN comprising three networks - a discriminator, a generator, and a feature extractor - that were updated concurrently. To achieve optimal GAN performance, we utilised the relativistic GAN loss as our objective function and introduced Gaussian noise to enhance the model's stability.

Specifically, the SISR model is trained using paired HR and LR inputs of the same subject, where the LR input is obtained by down-sampling the HR reference image by a fixed scale factor (*e.g.*, $\times 0.5$ down-sampling in our training). This is formulated as $I_{LR} = f(I_{HR})$, where $f(\cdot)$ denotes the downgrading function. In our case, we use linear down-sampling, which results in information loss. Therefore, the reverse process (*i.e.*, $g(\cdot) \approx f^{-1}(\cdot)$), known as the SR process, aims to recover high-resolution images from the LR images using a trained neural network in reference to the original HR images. The recovered SR image (\hat{I}_{SR}) is formulated as $\hat{I}_{SR} = g(I_{LR}) = f^{-1}(I_{LR})$. The reverse process $g(\cdot)$ is parameterized by a neural network, and the model continuously updates its parameters to learn the mapping between the

distribution of the downgraded LR samples and the training HR samples.

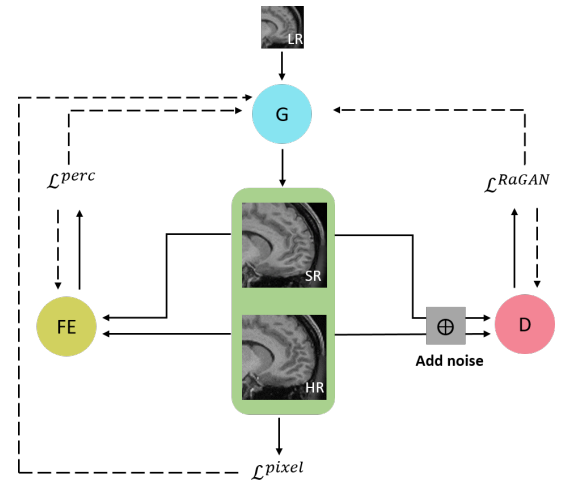


Fig. 2: Semantic diagram of our network during training. The discriminator, generator, and feature extractor are denoted as D, G, and FE respectively (see pseudo code in Algorithm 1). The *solid* arrow denotes image data flow, while the *dashed* arrow refers to the gradients which update the according networks; the *gray* block denotes adding instance noise to the SR and HR images, the *green* area denotes high-resolution image space. The low resolution(LR) MRI data is fed to the G network first, then SR MRI data is generated and is separately fed into D and FE networks. *Note:* our feature extractor network updates concurrently with the generator.

A. GAN Based SR Model

We use the GAN architecture to train the SR model, which contains a generator, a discriminator, and a feature extractor.

Typically, in a standard GAN, the input of the generator is a noise sample from a prior distribution, such as Gaussian distribution. However, in our context, the generator takes LR images as input and outputs super-resolution images, while the discriminator tries to distinguish between the generated images and the ground truth high-resolution images (see figure 2). In this paper, we utilise the following notations: D, G, FE represent the discriminator, generator, and feature extractor, respectively; ψ, θ, ϕ refer to the weight matrixes of their respective parameters.

The generator network in our architecture includes densely connected residual blocks, which facilitate efficient training, as well as sub-pixel layers [29] for up-sampling image dimensions. Meanwhile, the discriminator contains convolutional blocks with strided convolutional layers and instance normalization. In order to generate images with higher perceptual quality, we also incorporated a feature extractor that constrains the Euclidean distance between the SR and HR images. Our overall architecture can be viewed as a multi-player differential game [1], with the feature extractor acting as the third player, updated in an unsupervised manner instead of as a classifier. The gradient updates of the overall model are described in algorithm 1.

B. Densely Connected Residual Blocks

As the building block of the generator, we implemented densely connected residual blocks [11]. While many studies have used deeper architectures to extract more informative latent features, deep architectures can be prone to instability during training. This can cause vanishing or exploding gradients. To address this concern, [35] and [20] proposed to use densely connected residual blocks inside the generator models. This not only ensures the stability of the training but also improves the computational efficiency compared to generic ResNet [9].

C. Perceptual Loss

To ensure the perceptual fidelity of the SR, we propose to use a perceptual loss function (\mathcal{L}^{perc} in algorithm 1) to constrain the quality of SR results in feature space. The perceptual loss was first introduced in [16], where a pretrained VGG-19 network [30] was used to extract features. However, our implementation differs in that we do not use the pretrained VGG-19 network, but an actively updating ResNet10 network. More details are explained in the "Feature Matching" section below.

Our perceptual loss (\mathcal{L}^{perc} in algorithm 1) is defined as a l_1 loss in feature space, see equation (1). Here $I_{i,j,k}$ and $\hat{I}_{i,j,k}$ represent HR and SR intensity value at the i, j, k -th voxel in all three image dimensions (W, H, D), $\mathcal{F}(\cdot)$ represent the feature network.

$$\mathcal{L}^{perc} = \frac{1}{W \times H \times D} \sum_{i,j,k=1}^{W,H,D} |\mathcal{F}(I_{i,j,k}) - \mathcal{F}(\hat{I}_{i,j,k})| \quad (1)$$

As shown in [16], perceptual loss functions generally outperform MSE loss functions, because they better preserve the detailed texture of the image.

D. Relativistic Average GAN Loss

As a key factor to characterise the GAN dynamics, we use relativistic GAN loss [13] to make the training more efficient and stable. The standard GAN loss only discriminates between real and fake samples, but the relativistic average GAN loss function estimates how close the generated distribution is to the real distribution.

Compared to the standard GAN loss, which converges slower and suffers from instability, the relativistic GAN loss allows the model to converge faster and show better convergence stability. The discriminator is encouraged to distinguish real data as being more realistic than the average of the generated data. The real samples are denoted as $x \sim \mathbb{P}$, with \mathbb{P} the distribution of the real samples; the generated data are noted as $y \sim \mathbb{Q}$, with \mathbb{Q} the distribution of the generated samples. We propose to use the relativistic averaged discriminator (D_{Ra}), where $C(\cdot)$ is the critic network (i.e. discriminator without the last sigmoid function, $\tau(\cdot)$).

$$D_{Ra}(x, y) = \tau(C(x) - \mathbb{E}_{y \sim \mathbb{Q}} C(y)) \quad (2)$$

$$D_{Ra}(y, x) = \tau(C(y) - \mathbb{E}_{x \sim \mathbb{P}} C(x)) \quad (3)$$

The relativistic GAN loss for the discriminator (\mathcal{L}_D^{RaGAN}) and the generator (\mathcal{L}_G^{RaGAN}) is defined below. See also algorithm 1.

$$\begin{aligned} \mathcal{L}_D^{RaGAN}(x, y) = & -\mathbb{E}_{x \sim \mathbb{P}} [\log(D_{Ra}(x, y))] \\ & -\mathbb{E}_{y \sim \mathbb{Q}} [\log(1 - D_{Ra}(x, y))] \end{aligned} \quad (4)$$

$$\begin{aligned} \mathcal{L}_G^{RaGAN}(x, y) = & -\mathbb{E}_{x \sim \mathbb{P}} [\log(1 - D_{Ra}(y, x))] \\ & -\mathbb{E}_{y \sim \mathbb{Q}} [\log(D_{Ra}(y, x))] \end{aligned} \quad (5)$$

E. Instance Noise

As noted before, GANs suffer from convergence problems. Therefore we add linearly annealed Gaussian noise to the input of the discriminator to avoid early phase divergence, as proposed in [31].

Adding instance noise to both the generated SR samples and their reference samples before feeding them to the discriminator stabilises the training process. The main concept is to make the real and the generated distributions overlap by adding Gaussian noise. This has been shown to be an effective and computationally cheap way of balancing the GAN dynamics and ensuring convergence [31]. The expression for the discriminator can be rewritten as follows:

$$D(I + \epsilon, \hat{I} + \epsilon) \quad (6)$$

where $\epsilon \sim \mathcal{N}(0, \sigma)$ is the Gaussian noise with linearly decreasing variance from 1 to 0, with each update of the network gradients.

F. Feature Matching

In order to enhance the quality of generated samples, we employed feature matching, which involves updating the feature extractor network alongside the generator. This technique has been shown to improve the perceptual quality of images

Algorithm 1 Simultaneous gradient updating of our model. We use default values of learning rate $\gamma=0.0001$, coefficients of Adam optimiser $\beta_1 = 0.9$ and $\beta_2 = 0.999$, see section IV-B and figure 2.

Require: Initialise parameters, ψ, θ, ϕ , of D, G, FE with Kaiming initialization.

```

1: while not converge do
2:   Sample  $x \sim \mathbb{P}$ , a batch from the real images.
3:   Sample annealed noise  $\epsilon \sim \mathcal{N}(0, \sigma)$ , with standard deviation  $\sigma$  decreasing linearly from 1 to 0 per iteration.
4:    $\tilde{x}$  is from linearly down-sampling  $x$ . ▷ Simulating LR image  $\tilde{x}$ 
5:    $y \leftarrow G(\tilde{x})$  ▷ Generate SR image  $y$ 
6:    $\mathcal{L}^{pixel}(x, y) := |x - y|$ 
7:    $\mathcal{L}^{perc}(x, y) := |FE(x) - FE(y)|$ 
8:    $\phi \leftarrow \text{Adam}(\nabla_{\phi}[\mathcal{L}^{perc}(x, y)], \phi, \gamma, \beta_1, \beta_2)$  ▷ Update feature extractor
9:    $\theta \leftarrow \text{Adam}(\nabla_{\theta}[\mathcal{L}^{perc}(x, y) + \alpha\mathcal{L}^{pixel}(x, y) + \beta\mathcal{L}_G^{RaGAN}(x + \epsilon, y + \epsilon)], \theta, \gamma, \beta_1, \beta_2)$  ▷ Update generator
10:   $\psi \leftarrow \text{Adam}(\nabla_{\psi}[\mathcal{L}_D^{RaGAN}(x + \epsilon, y + \epsilon)], \psi, \gamma, \beta_1, \beta_2)$  ▷ Update discriminator
11: end while

```

in previous studies [12], [16]. Typically, a VGG-like network [30] is used as the feature extractor due to its pretrained ability to capture meaningful feature representations [35]. However, since we did not have access to any pre-trained networks for our application, we developed our own feature matching network.

We implemented a three-player game [1] where a feature extractor network is randomly initialised and updated alongside the generator. The gradient indirectly updates the feature extractor, with the objective function being the perceptual loss. The generator and feature extractor work in pairs to improve the perceptual quality of the image in an end-to-end manner. To serve as the feature extractor module, we utilized the lower layers of ResNet10 before the multi-perceptron layers, and updated its weights from random initialization during the GAN training.

While standard perceptual loss setups use the first 54 layers of a pre-trained VGG19 network for feature extraction [35], we found that ResNet10, a shallower architecture, performed better in our experiments when updated without pretraining. Additionally, when using the VGG-like feature extractor, we noticed that the generated images had undesirable checkerboard artefacts, which were not present when ResNet10 was used. Overall, the best quality of generated samples was achieved when concurrently updating ResNet10 with the generator to minimise the perceptual loss.

G. Objective Function

In order to generate images with both high perceptual quality and balanced training performance, we include \mathcal{L}_1 loss in the image domain, perceptual loss, and GAN loss as the overall objective function for the generator network. The parameters of the generator are constrained to learn both feature-wise (\mathcal{L}^{perc}) and image-wise (\mathcal{L}^{pixel}) representations of the ground truth, which the objective function seeks to minimise. The overall objective function of the generator is defined as:

$$\mathcal{L}_G = \mathcal{L}^{perc} + \alpha\mathcal{L}^{pixel} + \beta\mathcal{L}_G^{RaGAN} \quad (7)$$

where $\alpha = 0.01$ and $\beta = 0.005$ are empirical parameters for weighting image space \mathcal{L}_1 loss and Relativistic averaged GAN

loss.

The discriminator and the feature extracting networks are updated based on their respective loss, \mathcal{L}_D^{RaGAN} and \mathcal{L}^{perc} , as defined in equation(4) and equation(1).

IV. EXPERIMENTAL SETUP

A. Datasets

To test our approach, we used several datasets from different scanners, different imaging modalities or parts of body. Three of those datasets are part of the Human Connectome Project [34], the rest is from [28]. We name the datasets by the most distinguishable attribute of the each dataset, as described below.

Dataset "Insample": This dataset is downloaded from the *Lifespan Pilot Project*, as the part of the Human Connectome Project (HCP). It consists of T1-weighted (T1w) MRI images from 27 healthy subjects aged 8 to 75 (15 females) acquired in a Siemens 3T scanner. In our model we split them as 20 subjects for training and 7 for test. The resolution of the ground truth images is 0.8mm isotropic, with matrix size of $208 \times 300 \times 320$.

Dataset "Contrast": This dataset is also from the *Lifespan Pilot Project* described above, but now we use the T2-weighted(T2w) images of the same subjects.

Dataset "Resolution": This test dataset consists of 1113 T1w brain MRI images, from the WU-Minn Young Adult study of the HCP, acquired in the 3T scanner at the resolution of 0.7mm isotropic.

Dataset "Knee": This dataset contains 20 knee MRI proton density weight images downloaded from [28].

B. Implementation Details

In the implementation of the network, we trained a generator network, a critic network, and a feature extractor network. The generator network consists of 3 Residual-in-Residual Dense Blocks [35], which are embedded densely connected residual units, without any batch norm layer. The critic network is the same as a discriminator without the final non-linear activation layer. The feature extractor uses convolutional layers of ResNet10 before linear layers. All three networks

are initialised by Kaiming initialization [8] and are optimised by Adam optimizer [15], using coefficients of $\beta_1 = 0.9$, $\beta_2 = 0.999$, and learning rate of $\gamma = 10^{-4}$. The variance of the instance noise decreases linearly in each iteration, from $\sigma = 1$ to 0. The training simultaneously updates, on PyTorch framework [25], a feature extractor, a generator and a discriminator network for 60000 iterations, on a NVIDIA’s Ampere 100 GPU.

C. Evaluation Metrics

Several metrics have been proposed for measuring the accuracy of super-resolution results, for example, Structure-Similarity-Index-Measurement (SSIM), Peak-Signal-Noise-Ratio (PSNR), and Normalized-Root-Mean-Square-Error (NRMSE). However, these metrics sometimes do not reflect image fidelity correctly [21], [38]. Since SISR is considered an ill-posed problem, these measurements only reveal the statistical similarity between the target and the reference, which are imprecisely high when the target is blurry so that the mean and variance of the target fit the ground truth better [21]. Therefore, here we also used Learned-Perceptual-Image-Patch-Similarity (LPIPS) metrics which better capture perceptual similarity [38]. Here we use the 2D slice-wise implementation provided by [38].

Perceptual metrics such as LPIPS have been pretrained on large image datasets and are known to extract meaningful features that closely resemble human visual quality [21], [38]. However, unlike traditional metrics such as PSNR and SSIM, LPIPS may not always correlate with them.

V. RESULTS

A. Experiment 1: Insample Super-Resolution

The first experiment is to test in-sample super-resolution using *Dataset "Insample"*. Due to the memory constraints, we split the images into overlapping patches of size $64 \times 64 \times 64$, which are defined by sliding a window in step size 16 along each dimension with zero-padding at the end. For each subject, 2160 patches with overlapping patches were obtained as training data. To simulate lower-resolution images, LR patches were obtained by linearly down-sampling HR patches to half of their original resolution, namely to a resolution of $1.6mm$ with a matrix size of $32 \times 32 \times 32$. The paired patches of LR and HR images were fed into the model for training.

For comparison, we tested our approach against three competing approaches, namely ESRGAN [35], ArSSR [36], and DCSRN [3]. ESRGAN was only available in 2D, and we reconfigure it in 3D and retrained it on a 3D dataset. Specifically, we pretrained the first 54 layers of a 3D VGG-19 network on 3D MRI images. Both the ArSSR and DCSRN models are available in 3D, but we re-trained the model on *Dataset "Insample"*.

The results are shown in figure1. Note that our model recovered the ground truth best, especially with regard to small blood vessels (subfigure1e); our model also recovered very detailed cerebellum structures (second and third row of figure1). The quantitative results are shown in tableI. Note that our method outperformed other models in NRMSE and LPIPS.

Model	PSNR \uparrow	SSIM \uparrow	NRMSE \downarrow	LPIPS(2D) \downarrow
Tri-linear	33.038	0.876	0.023	0.084
ESRGAN-3D	37.022	0.933	0.013	0.044
DCSRN	37.635	0.954	0.013	0.052
ArSSR	28.038	0.280	0.048	0.291
<i>ours</i>	36.922	0.943	0.013	0.040

TABLE 1: Quantitative comparison of performance among the *state-of-the-art* models on *dataset "Insample"*, where \uparrow indicates the higher the value the better the image quality, *vice versa* for \downarrow . Note: the sharpness and LPIPS value better represent image visual quality in accordance to the figure4.

B. Experiment 2: Small Training Samples

In this experiment, we trained our model on *Dataset "Insample"* using only one image for training. Here we compared the performance of models trained on 1 and 20 subjects, the qualitative performance of the 1 subject-trained model is on par with the 20 subject-trained one as is shown in figure3.

Owing to the common properties of brain MRI, which contains less informative background and relatively less heterogeneous sample contents, convolutional neural networks can efficiently learn meaningful feature representations of brain MRI patches for SR tasks [39]. Given that we assume it is possible for a 3D convolutional neural network to learn strong enough inductive bias towards SISR, using a limited amount of training samples.

Our model utilizes the relativistic GAN and feature matching techniques to significantly improve efficiency. This intrinsic property of brain MRI data means that fewer training samples are required compared to common 2D vision tasks, making it possible to reduce the amount of training data needed for the brain MRI model. Empirically, we demonstrate that it is possible to address the data deficiency issue for MRI SR by training our model on just one subject. Interestingly, we observe that the generator’s performance is not sensitive to the number of training samples when using the feature extractor network, such as ResNet10. Furthermore, during our experiments, we found that a deeper architecture used for feature matching does not outperform a shallower one. For instance, ResNet50 performs worse than using ResNet10 as a feature extractor.

We noticed the performance of the generator is not sensitive to the numbers of the training samples, when using the feature extractor network(e.g. ResNet10). Besides, the deeper architecture used for feature matching does not perform better than a shallow one during our experiment (e.g. ResNet50 performs worse than using ResNet10 as feature extractor).

C. Experiment 3: Zero-Shot Inference on OOD Data

In our out-of-distribution experiment, we trained our model using the Dataset "Insample" and evaluated its performance on three different datasets: "Contrast", "Resolution", and "Knee". The ground truth of these OOD datasets exhibits significant variations in terms of contrast, resolution, and body part, as are shown in figure4 and 5.

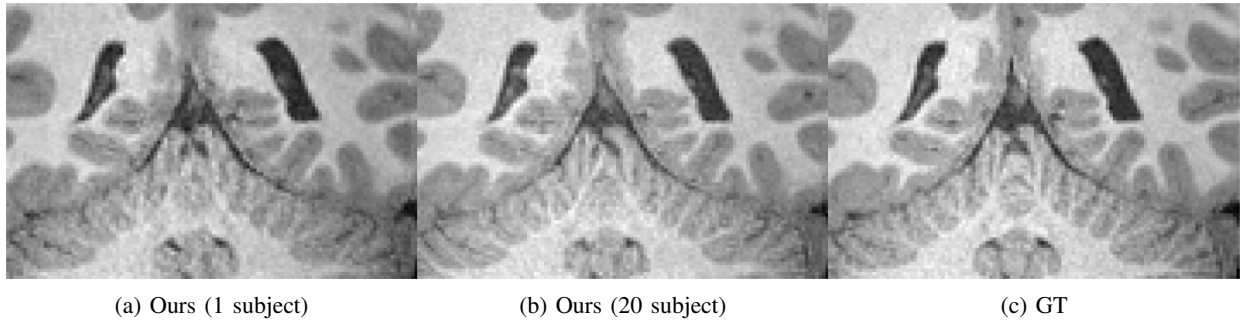


Fig. 3: Effect of training dataset size on the quality of super-resolution (SR) images. From *left to right* are the zoom-in views of the SR images generated by the models trained on: 1 subject, 20 subjects, and ground truth. *Note:* The brain structure is mostly preserved in all subfigures except for the contrast change in subfigure(a). Our proposed model achieves better perceptual quality in the cerebellum when trained on 20 subjects in subfigure(b), indicating only slight improvement in SR quality with an increase in training samples

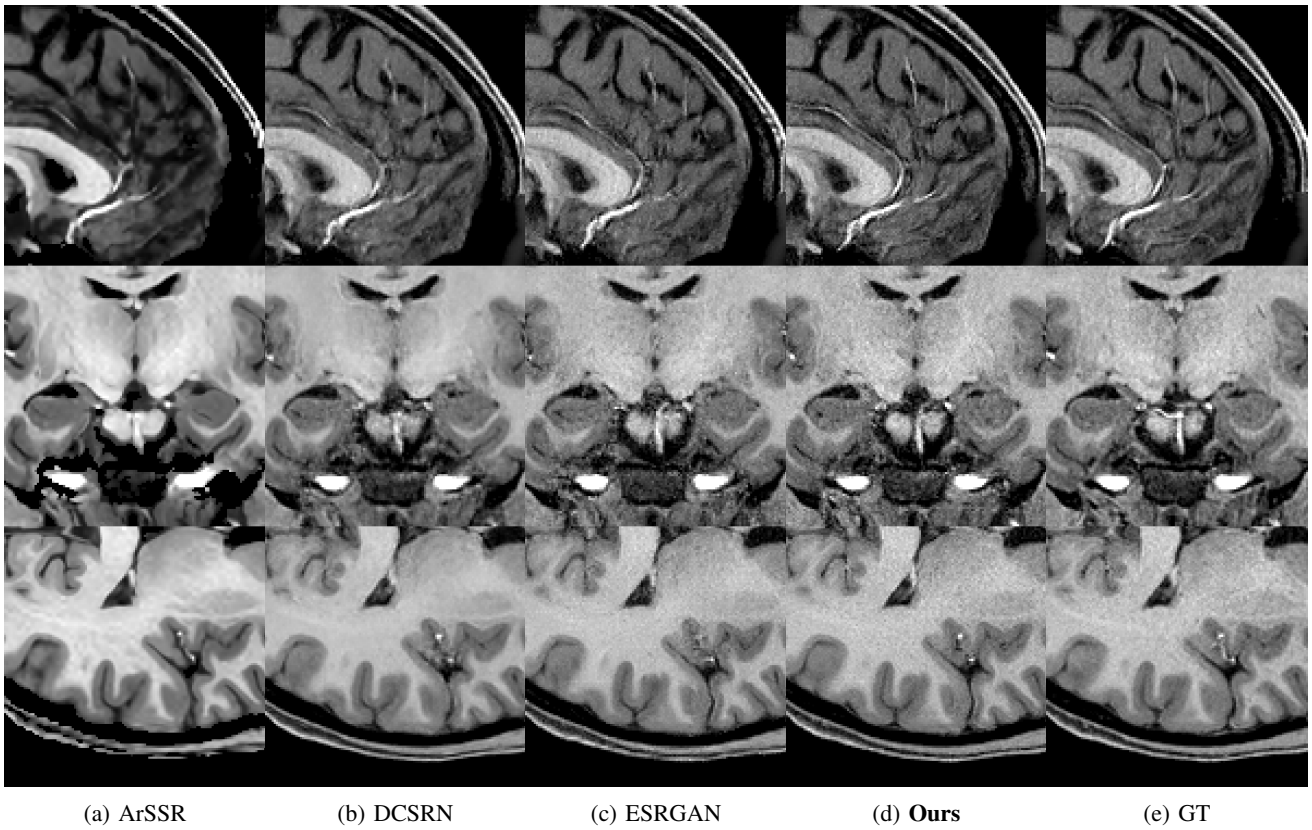


Fig. 4: Qualitative comparison on dataset "Resolution" among zoom-in SR results with different perceptual quality. (a)-(e) shows visual comparison in a zoom-in view of SR results, in *Dataset "Resolution"*: ArSSR, DCSRN, ESRGAN, **Ours**, and GT. *Note:* Our result shows the best quality visually and a lowest LPIPS score, despite of having low PSNR and SSIM score.

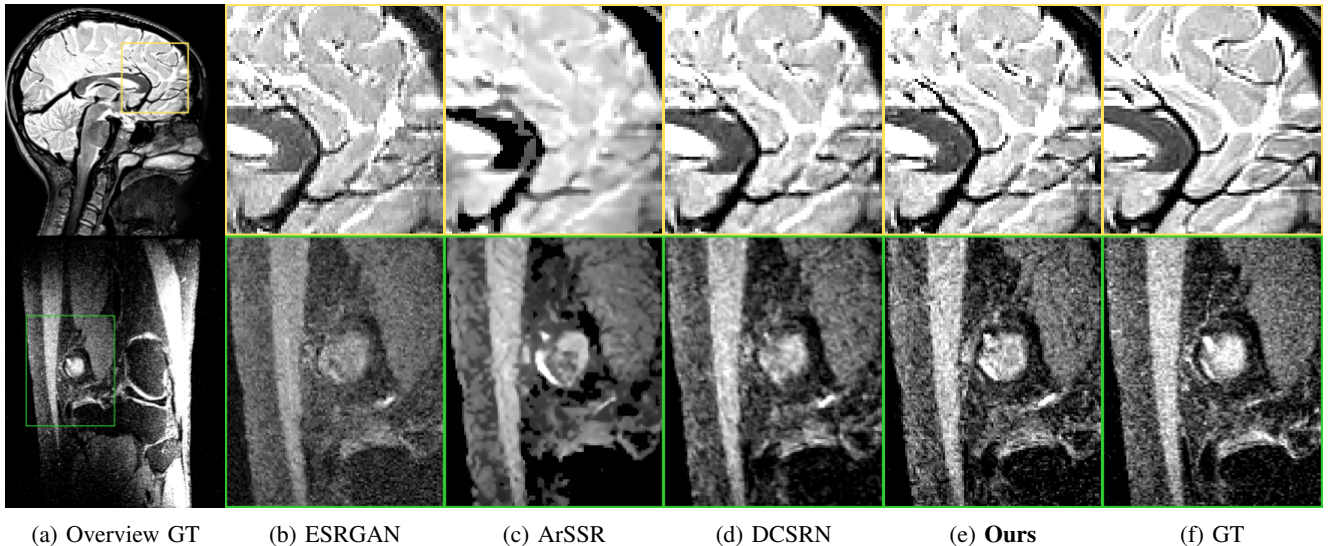


Fig. 5: Qualitative comparison on out-of-distribution datasets "Contrast" and "Knee" for different models. Each column shows: (a) overall view of GT image and (b)-(f) zoom-in SR results of ESRGAN [35], ArSSR [36], DCSRN [3], **Ours**, and ground truth; The *top* row shows the SR results of models tested on brain MRI images with T2w contrast from dataset "Contrast". Our model produces the most accurate vessel structures.; the *bottom* row shows the SR results of the models tested on knee MRI images with PDw contrasts from dataset "Knee". Our model outperformed the other models in reconstructing detailed knee joint and surrounding tissue structures.

For comparison purposes, we also tested ESRGAN, DCSRN, and ArSSR, trained on the dataset "Insample", on these OOD tasks. Our model outperformed the other models in this experiment on all three datasets, by best producing image details that most closely approximated the GT.

Our model performed better in recovering the details of vessels in the sagittal plane of the SR image, as shown in the top row of figure 4 on the "Resolution" dataset. In contrast, other models, such as ArSSR and DCSRN, produced over-smoothed images, while ESRGAN produced images with noisy details. Our model also exhibited superior image quality on the "Contrast" and "Knee" datasets, where it closely approximated the blood vessels and the round-shaped bone structure, as demonstrated in subfigure 5e.

Although DCSRN obtained the highest PNSR and SSIM, the LPIPS score of our model was well aligned with its image quality and details, as demonstrated in figure 4 and table I and II.

Model	PSNR \uparrow	SSIM \uparrow	NRMSE \downarrow	LPIPS \downarrow
ESRGAN-3D(20 subj)	37.181	0.957	0.013	0.039
DCSRN(1 subj)	37.420	0.959	0.013	0.088
DCSRN(20 subj)	37.564	0.962	0.013	0.051
ours(1 subj)	36.355	0.953	0.014	0.048
ours(20 subj)	36.922	0.953	0.013	0.038

TABLE II: Quantitative comparison of robustness among the *state-of-the-art* models on *Dataset "Resolution"*.

Our experiments showed that our approach can be generalized to different datasets with little decrease in performance. Notably, even when exposed to vastly different contrast or anatomy, our model did not collapse into specific training data

and generalized well on out-of-distribution datasets.

VI. DISCUSSION

In this paper, an effective method is proposed for stabilizing GAN training, which outperforms *state-of-the-art* models in SR tasks on 3D brain MRI data. Our approach involves adding Gaussian noise to discriminator inputs, using a three-player GAN model, and applying the relativistic GAN loss as the objective function. Our experimental results demonstrate that this method can ensure effective training convergence and achieve better generalizability. Several key findings are presented in this paper. First, the proposed model generates SR results with superior perceptual quality compared to existing methods, even when the amount of training data is small. Secondly, the model achieves accurate SR generation and convergence even when trained on a single subject. Finally, the model exhibits strong generalizability and is less prone to overfitting, as evidenced by its successful performance on previously unseen datasets (*i.e.* *Dataset "Contrast"*, *Dataset "Resolution"*, and *Dataset "Knee"*).

While the LPIPS score is a reliable metric for assessing the perceptual quality of images, it is primarily designed for 2D image evaluation and may overlook information in the cross-plane of volumetric MRI. Therefore, future research should focus on developing specialized methods for evaluating the perceptual quality of 3D MRI images.

REFERENCES

- [1] David Balduzzi, Sebastien Racaniere, James Martens, Jakob Foerster, Karl Tuyls, and Thore Graepel. The mechanics of n-player differentiable games. In Jennifer Dy and Andreas Krause, editors, *Proceedings of the 35th International Conference on Machine Learning*, volume 80 of *Proceedings of Machine Learning Research*, pages 354–363. PMLR, 10–15 Jul 2018. 4, 5

- [2] Andrew Brock, Jeff Donahue, and Karen Simonyan. Large scale GAN training for high fidelity natural image synthesis. In *International Conference on Learning Representations*, 2019. 2
- [3] Yuhua Chen, Yibin Xie, Zhengwei Zhou, Feng Shi, Anthony G. Christodoulou, and Debiao Li. Brain MRI super resolution using 3d deep densely connected neural networks. In *2018 IEEE 15th International Symposium on Biomedical Imaging (ISBI 2018)*. IEEE, apr 2018. 1, 2, 3, 6, 8
- [4] Chao Dong, Chen Change Loy, Kaiming He, and Xiaoou Tang. Learning a deep convolutional network for image super-resolution. In *Computer Vision – ECCV 2014*, pages 184–199, Cham, 2014. Springer International Publishing. 1, 2
- [5] Alexey Dosovitskiy, Lucas Beyer, Alexander Kolesnikov, Dirk Weissenborn, Xiaohua Zhai, Thomas Unterthiner, Mostafa Dehghani, Matthias Minderer, Georg Heigold, Sylvain Gelly, Jakob Uszkoreit, and Neil Houlsby. An image is worth 16x16 words: Transformers for image recognition at scale. In *International Conference on Learning Representations*, 2021. 1, 2
- [6] Ian Goodfellow, Jean Pouget-Abadie, Mehdi Mirza, Bing Xu, David Warde-Farley, Sherjil Ozair, Aaron Courville, and Yoshua Bengio. Generative adversarial nets. In Z. Ghahramani, M. Welling, C. Cortes, N. Lawrence, and K.Q. Weinberger, editors, *Advances in Neural Information Processing Systems*, volume 27. Curran Associates, Inc., 2014. 1, 3
- [7] Ishaan Gulrajani, Faruk Ahmed, Martin Arjovsky, Vincent Dumoulin, and Aaron C Courville. Improved training of wasserstein gans. In *Advances in Neural Information Processing Systems*, volume 30. Curran Associates, Inc., 2017. 1, 2, 3
- [8] Kaiming He, Xiangyu Zhang, Shaoqing Ren, and Jian Sun. Delving deep into rectifiers: Surpassing human-level performance on imagenet classification. In *Proceedings of the IEEE International Conference on Computer Vision (ICCV)*, December 2015. 6
- [9] Kaiming He, Xiangyu Zhang, Shaoqing Ren, and Jian Sun. Deep residual learning for image recognition. In *2016 IEEE Conference on Computer Vision and Pattern Recognition (CVPR)*, pages 770–778, 2016. 2, 4
- [10] Jonathan Ho, Ajay Jain, and Pieter Abbeel. Denoising diffusion probabilistic models. In H. Larochelle, M. Ranzato, R. Hadsell, M.F. Balcan, and H. Lin, editors, *Advances in Neural Information Processing Systems*, volume 33, pages 6840–6851, 2020. 1
- [11] G. Huang, Z. Liu, L. van der Maaten, and K.Q. Weinberger. Densely Connected Convolutional Networks. In *Proceedings of the IEEE Conference on Computer Vision and Pattern Recognition (CVPR)*, July 2017. 4
- [12] Justin Johnson, Alexandre Alahi, and Li Fei-Fei. Perceptual losses for real-time style transfer and super-resolution, 2016. 2, 5
- [13] Alexia Jolicœur-Martineau. The relativistic discriminator: a key element missing from standard GAN. In *International Conference on Learning Representations*, 2019. 1, 2, 4
- [14] Jiwon Kim, Jung Kwon Lee, and Kyoung Mu Lee. Accurate image super-resolution using very deep convolutional networks. In *The IEEE Conference on Computer Vision and Pattern Recognition (CVPR Oral)*, June 2016. 1, 2
- [15] Diederik P. Kingma and Jimmy Ba. Adam: A method for stochastic optimization. In *3rd International Conference on Learning Representations, ICLR 2015, San Diego, CA, USA, May 7-9, 2015, Conference Track Proceedings*, 2015. 6
- [16] C. Ledig, L. Theis, F. Huszar, J. Caballero, A. P. Aitken, A. Tejani, J. Totz, Z. Wang, and W. Shi. Photo-realistic single image super-resolution using a generative adversarial network. *CoRR*, abs/1609.04802, 2016. 1, 2, 4, 5
- [17] Chongxuan Li, Kun Xu, Jun Zhu, and Bo Zhang. Triple generative adversarial nets. In *Proceedings of the 31st International Conference on Neural Information Processing Systems, NIPS’17*, page 4091–4101. Curran Associates Inc., 2017. 1
- [18] Guangyuan Li, Jun Lv, Yapeng Tian, Qi Dou, Chengyan Wang, Chenliang Xu, and Jing Qin. Transformer-empowered multi-scale contextual matching and aggregation for multi-contrast mri super-resolution. In *2022 IEEE/CVF Conference on Computer Vision and Pattern Recognition (CVPR)*, pages 20604–20613, 2022. 2
- [19] Zhisheng Lu, Juncheng Li, Hong Liu, Chaoyan Huang, Linlin Zhang, and Tiejong Zeng. Transformer for single image super-resolution. In *Proceedings of the IEEE/CVF Conference on Computer Vision and Pattern Recognition (CVPR) Workshops*, pages 457–466, June 2022. 2
- [20] Cheng Ma, Yongming Rao, Yean Cheng, Ce Chen, Jiwen Lu, and Jie Zhou. Structure-preserving super resolution with gradient guidance. In *Proceedings of the IEEE Conference on Computer Vision and Pattern Recognition (CVPR)*, 2020. 2, 4
- [21] Chao Ma, Chih-Yuan Yang, Xiaokang Yang, and Ming-Hsuan Yang. Learning a no-reference quality metric for single-image super-resolution. *Computer Vision and Image Understanding*, 158:1–16, 2017. 6
- [22] Arjovsky Martin, Chintala Soumith, and Bottou Léon. Wasserstein generative adversarial networks. In Doina Precup and Yee Whye Teh, editors, *Proceedings of the 34th International Conference on Machine Learning*, volume 70 of *Proceedings of Machine Learning Research*, pages 214–223. PMLR, 06–11 Aug 2017. 1, 2, 3
- [23] Lars Mescheder, Sebastian Nowozin, and Andreas Geiger. Which training methods for gans do actually converge? In *International Conference on Machine Learning (ICML)*, 2018. 1, 2, 3
- [24] Takeru Miyato, Toshiki Kataoka, Masanori Koyama, and Yuichi Yoshida. Spectral normalization for generative adversarial networks. In *International Conference on Learning Representations*, 2018. 2
- [25] Adam Paszke, Sam Gross, Francisco Massa, Adam Lerer, James Bradbury, Gregory Chanan, Trevor Killeen, Zeming Lin, Natalia Gimelshein, Luca Antiga, Alban Desmaison, Andreas Köpf, Edward Yang, Zach DeVito, Martin Raison, Alykhan Tejani, Sasank Chilamkurthy, Benoit Steiner, Lu Fang, Junjie Bai, and Soumith Chintala. Pytorch: An imperative style, high-performance deep learning library, 2019. 6
- [26] Chi-Hieu Pham, Aurélien Ducournau, Ronan Fablet, and François Rousseau. Brain mri super-resolution using deep 3d convolutional networks. In *2017 IEEE 14th International Symposium on Biomedical Imaging (ISBI 2017)*, pages 197–200, 2017. 1, 2
- [27] Chitwan Saharia, Jonathan Ho, William Chan, Tim Salimans, David J Fleet, and Mohammad Norouzi. Image super-resolution via iterative refinement. *arXiv:2104.07636*, 2021. 2
- [28] Anne Marie Sawyer, Michael Lustig, Marcus Alley, Phdmartin Uecker, Patrick Virtue, Peng Lai, and Shreyas Vasanawala. Creation of fully sampled MR data repository for compressed sensing of the knee. In *In Proceedings of Society for MR Radiographers & Technologists (SMRT) 22nd Annual Meeting, Salt Lake City, UT, USA, 2013*. 5
- [29] Wenzhe Shi, Jose Caballero, Ferenc Huszar, Johannes Totz, Andrew P. Aitken, Rob Bishop, Daniel Rueckert, and Zehan Wang. Real-time single image and video super-resolution using an efficient sub-pixel convolutional neural network. In *Proceedings of the IEEE Conference on Computer Vision and Pattern Recognition (CVPR)*, June 2016. 4
- [30] Karen Simonyan and Andrew Zisserman. Very deep convolutional networks for large-scale image recognition. In Yoshua Bengio and Yann LeCun, editors, *3rd International Conference on Learning Representations, ICLR 2015, San Diego, CA, USA, May 7-9, 2015, Conference Track Proceedings*, 2015. 4, 5
- [31] Casper Kaae Sønderby, Jose Caballero, Lucas Theis, Wenzhe Shi, and Ferenc Huszar. Amortised MAP inference for image super-resolution. In *5th International Conference on Learning Representations, ICLR 2017, Toulon, France, April 24-26, 2017, Conference Track Proceedings*. OpenReview.net, 2017. 3, 4
- [32] Yang Song and Stefano Ermon. Generative modeling by estimating gradients of the data distribution. In H. Wallach, H. Larochelle, A. Beygelzimer, F. d’Alché-Buc, E. Fox, and R. Garnett, editors, *Advances in Neural Information Processing Systems*, volume 32. Curran Associates, Inc., 2019. 1, 2
- [33] Yao Sui, Onur Afacan, Ali Gholipour, and Simon K. Warfield. Learning a gradient guidance for spatially isotropic mri super-resolution reconstruction. In Anne L. Martel, Purang Abolmaesumi, Danaïl Stoyanov, Diana Mateus, Maria A. Zuluaga, S. Kevin Zhou, Daniel Racoceanu, and Leo Joskowicz, editors, *Medical Image Computing and Computer Assisted Intervention – MICCAI 2020*, pages 136–146, Cham, 2020. Springer International Publishing. 1, 2
- [34] D.C. Van Essen, S.M. Smith, D.M. Barch, T.E.J. Behrens, E. Yacoub, and K. Ugurbil. The WU-Minn Human Connectome Project: An overview. *NeuroImage*, 80(64-79), 2013. 5
- [35] X. Wang, K. Yu, S. Wu, J. Gu, Y. Liu, C. Dong, Y. Qiao, and C. Loy. ESRGAN: Enhanced super-resolution generative adversarial networks. In *The European Conference on Computer Vision Workshops (ECCVW)*, September 2018. 1, 2, 3, 4, 5, 6, 8
- [36] Qing Wu, Yuwei Li, Yawen Sun, Yan Zhou, Hongjiang Wei, Jingyi Yu, and Yuyao Zhang. An arbitrary scale super-resolution approach for 3d mr images via implicit neural representation. *IEEE Journal of Biomedical and Health Informatics*, pages 1–12, 2022. 1, 2, 3, 6, 8
- [37] Kun Xu, Chongxuan Li, Jun Zhu, and Bo Zhang. Understanding and stabilizing GANs’ training dynamics using control theory. In *Proceedings of the 37th International Conference on Machine Learning*, volume 119 of *Proceedings of Machine Learning Research*, pages 10566–10575. PMLR, 13–18 Jul 2020. 1, 2, 3
- [38] Richard Zhang, Phillip Isola, Alexei A Efros, Eli Shechtman, and Oliver Wang. The unreasonable effectiveness of deep features as a perceptual metric. In *CVPR*, 2018. 6
- [39] Yulun Zhang, Kai Li, Kunpeng Li, and Yun Fu. Mr image super-resolution with squeeze and excitation reasoning attention network. In

2021 *IEEE/CVF Conference on Computer Vision and Pattern Recognition (CVPR)*, pages 13420–13429, 2021. [2](#), [6](#)

- [40] Yulun Zhang, Kunpeng Li, Kai Li, Lichen Wang, Bineng Zhong, and Yun Fu. Image super-resolution using very deep residual channel attention networks. In *ECCV*, 2018. [2](#)